Statistical properties of flux closure induced by solar wind dynamic pressure fronts.

B. Hubert[(1)], C. Blockx[(1)] , S.E. Milan[(2)], S.W.H. Cowley[(2)]

1. Laboratory for Planetary and Atmospheric Physics, University of Liège, Belgium
2. Department of Physics & Astronomy, University of Leicester, Leicester LE1 7RH, UK

J. Geophys. Res., 114, A07211, doi:10.1029/2008JA013813.

Abstract

We present a statistical study of flux closure intervals induced by solar wind dynamic pressure fronts. We consider that a dynamic pressure front reaches the Earth when a dayside subauroral proton flash is observed in the SI2 channel of the IMAGE-FUV experiment. This pragmatic criterion selects both weak and strong pressure fronts. It is found that the preconditioning of the magnetosphere prior to the pressure pulse arrival mainly governs the magnetospheric response to a weak solar wind dynamic pressure front. This preconditioning includes the amount of open magnetic flux available in the magnetosphere prior to the pressure front arrival and the size of the magnetospheric cavity. However, in the case of a strong pressure pulse, the magnetospheric response is more sensitive to the solar wind properties characterizing the dynamic pressure front. Not only is the pressure jump important, but also the variation of the solar wind velocity and IMF magnitude. In overall terms, we find that a strong dynamic pressure front is typically characterized by a dynamic pressure increase larger than ~2.8 nPa that takes place on time scales of the order of a few minutes.

1. Introduction

The solar wind is the plasma outflow from the solar atmosphere. It carries the interplanetary magnetic field (IMF), which is frozen in the solar plasma. When the solar wind reaches the Earth, the geomagnetic field and the IMF can interconnect, and create open magnetic flux, that consists of magnetic field lines that originate in the interior of the planet and close through the interplanetary medium. The solar wind reaches the planet at a velocity larger than the characteristic wave speed (the speed of magnetosonic waves), so that a bow shock envelopes the magnetic environment of the planet, at a typical standoff distance of ~15 Earth radii (R_E) upstream from the planet in the subsolar region. The pressure exerted by the solar wind on the Earth's magnetosphere compresses it on the dayside, and gives it an elongated shape, creating the magnetotail on the nightside. Newly opened field lines, created on the dayside, are convected antisunward towards the magnetotail where they eventually undergo another reconnection process that closes them again, thus reconfiguring the magnetic topology back to a more dipolar pattern, releasing the energy that regularly powers the substorm expansion phase. Occasionally, the Sun releases a burst of material, creating a discontinuity in the solar wind, that translates to an increased dynamic pressure, either due to the increased plasma density or to an enhanced velocity (or both), the most spectacular of which is the coronal mass ejection (CME), i.e. an explosive process that releases large quantities of solar material into space. When a solar wind pressure front reaches the Earth, it compresses the magnetosphere, and sometimes triggers a substorm expansion phase, during which a large amount of open flux is closed in the magnetotail.

Boudouridis et al. [2003, 2004] showed that the interaction of the magnetosphere with solar wind dynamic pressure pulse results in a sharp reduction in the polar cap size, a clear signature of flux closure, especially when a pressure pulse hits the magnetosphere after an interval of southward IMF, i.e. after the magnetosphere has been loaded with open flux by magnetic reconnection on the dayside. *Brittnacher et al.* [2000] observed an auroral intensification triggered by a CME which develops from the dayside oval and propagates towards the nightside. *Meurant et al.* [2003, 2004] showed that solar wind dynamic pressure pulses can trigger an enhancement of auroral activity, in agreement with *Boudouridis et al.* [2003]. They showed that this enhancement is stronger for southward IMF conditions. For the set of events studied by *Meurant et al.* [2004], the preconditioning of the magnetosphere was found to be less important than the properties of the solar wind during the pressure pulse. In particular, they found that the auroral response is stronger for larger IMF intensity and solar wind speed. It was also shown that the propagation of the auroral brightening from the dayside to the nightside occurred sooner for the proton aurora than for the electron aurora [*Meurant et al.*, 2003]. Moreover, compression of the dayside magnetosphere first results in the formation of a dayside subauroral proton flash [*Hubert et al.*, 2003]. It was also shown that the compression of the magnetotail by a solar wind dynamic pressure pulse can also directly stimulate magnetic flux closure because it creates the conditions necessary for magnetic reconnection in the tail [*Hubert et al.*, 2006b] as the pressure disturbance propagates all the way down to the plasma sheet. *Meurant et al.* [2005] showed that pressure pulse-induced and isolated substorms largely share the same properties, the pulse being the trigger that initiates the reconfiguration of the unstable magnetosphere.

We have developed a method that combines ground based data from the Super Dual Auroral Radar Network (SuperDARN) and global images of the proton aurora from the Spectrographic Imager at 121.8 nm (SI12) onboard the Imager for Magnetosphere to Aurora Global Exploration (IMAGE) satellite [*Mende et al.*, 2000a, b] in order to estimate the magnetospheric open flux and the opening and closure rates of magnetic flux [*Hubert et al.*, 2006a]. These rates are expressed as voltages according to Faraday's law.

In the present study, we analyse the relation between the properties of solar wind pressure pulses and the magnetospheric response in terms of open flux storage and closure. In particular, we search for correlations between the properties of the solar wind and the opening and closure of magnetic flux. The configuration of the geomagnetic field is also considered using geosynchronous data from the GOES satellites. The role of preconditioning of the magnetospheric system is considered as well. Throughout the text, we will interchangeably use the terms (solar wind) dynamic pressure front or pulse, pressure front or pulse, or simply front or pulse to designate a solar wind dynamic pressure pulse.

2. Data Availability and Selection

As already outlined in the introduction, the amount of open flux is estimated using data from the SI12 instrument of the FUV experiment onboard the IMAGE satellite [*Hubert et al., 2006a*]. This instrument produces global images of the Doppler shifted Lyman-α emission, which is solely due to the precipitation of auroral protons, and is used here to estimate the location of the open/closed field line boundary (ocb) at ionospheric altitude, as well as its motion. The SuperDARN radar network measures the ionospheric convection, and allows the reconstruction of the ionospheric electric field [*Ruohoniemi and Baker,* 1998; *Cowley and Lockwood* 1992]. The SI12 data are used in combination with the SuperDARN radar data to estimate the opening and closure voltages that characterise the variations of the amount of open flux. The solar wind data are from the ACE satellite. We found 68 cases of pressure pulses over the period from June 2000 to February 2002, for which ACE, SI12 and SuperDARN data were available. Instead of identifying the pressure pulses from a criterion based on variations of the solar wind dynamic pressure, we identified dynamic pressure pulses from a more pragmatic standpoint. It has been shown that, when a solar wind pressure pulse reaches the Earth, it compresses the dayside magnetosphere in such a manner that it stimulates the precipitation of protons along closed field lines that map to the dayside ionosphere at magnetic latitudes lower than that of the auroral oval, creating a dayside subauroral proton flash [*Hubert et al.,* 2003*; Fuselier et al.,* 2004]. We searched the SI12 dataset for dayside subauroral proton flash signatures, and we checked a posteriori that there was actually an increase of the solar wind dynamic pressure in the ACE solar wind data, when available. This pragmatic approach also has the advantage of reducing the uncertainty in the time of propagation of the solar wind feature from the ACE location to the Earth's magnetosphere, especially if we consider that a shock wave (or any disturbance) propagates within the medium in addition to being advected along with the plasma motion. Moreover, in the case of weak pressure pulses, we can be sure that the solar wind pressure front did actually interact with the magnetosphere. For these weak pressure pulses, the identification of the pressure increase responsible for the proton flash was sometimes more difficult, and there remains some uncertainty in a few cases. The method of selection of pressure pulse-events led us to select more than 85 cases of dynamic pressure fronts. Some of them had to be excluded because of a failure of our open/closed boundary identification software, especially when the viewing conditions were not good enough or when the proton aurora was too dim, leaving us with 68 cases.

The duration of the interval that we investigate after the arrival of a particular pressure front is again determined from a pragmatic standpoint: the interaction of the pressure front with the magnetosphere generally stimulates an intensification of the flux closure voltage (sometimes minor). The end of the interval that we consider is chosen to be the time at which the closure voltage returns to a value close to its initial level prior to the front arrival (i.e. within 10 kV), with a maximum duration limited to 35 minutes. In exceptional cases when the intensification of the closure voltage is so weak that it remains under 10 kV, a duration of 20 min is chosen. As an example, **Figure 1** shows the solar wind properties, the open flux, the opening and closure voltages, and the net reconnection voltage obtained on 4 November 2000. As the nightside (dayside) reconnection voltage represents a decrease (an increase) of the open flux, we choose to express the nightside flux closure (dayside flux opening) rate as a negative (positive, respectively) voltage, so that the net voltage, i.e. the sum of the opening and closure voltages, represents the time derivative of the open flux. A sharp dynamic pressure front was observed by the ACE satellite shortly after 0130 UT. This front reached the Earth and triggered a dayside subauroral proton flash detected by the SI12 instrument at 0224 UT (vertical dotted line). The open magnetic flux deduced from the SI12 observations prior to the dynamic pressure pulse arrival was rather low (~ 0.46 GWb), a situation compatible with the northward IMF orientation. The closure voltage estimated from the SI12 and SuperDARN observations intensified after the dynamic pressure pulse arrived at the planet and reached ~ -125 kV. The closure voltage returned to pre-pulse values after ~35 min. Note that, as time smoothing has to be applied to correctly estimate the reconnection voltages, in an absolute sense, our resolution is not the cadence of image acquisition of the FUV-SI12 instrument (i.e. ~2 min) but only ~12-14 min. This results in a smearing of the pulse signature in the closure voltage curve, so that the striking time coincidence between the very sharp signature in the slope of V_{cl} and the pressure front arrival can be considered incidental: although the pressure pulse arrival generally initiates an intensification of the flux closure, the signature in the closure voltage curve is generally not that sharp right at the time of the arrival of the solar wind dynamic pressure pulse.

Several quantities can be determined that, potentially, can reveal the nature of the interaction between interplanetary shocks (dynamic pressure fronts in this study) and the magnetosphere. The amount of open flux itself is of course considered, but its variations can also be important: the net variation of the open flux, its maximum rate of change during the whole event and during the interaction of the magnetosphere with the ramp of the solar wind pressure front, and its initial value are all physical quantities to be studied as well. A similar study of the flux closure rate can also be undertaken: its average, initial, and maximal values must be considered (maximum in terms of its absolute value, i.e. the minimal value of the closure voltage, which is a negative number). The net intensification and rate of change of the closure voltage has also to be considered. In addition, the time integral of the closure voltage is also computed. It represents the total amount of open flux that goes through closure during the interval, whereas the variation of the amount of open flux during the interval includes a flux opening contribution from the dayside reconnection site.

The solar wind data can also be used to determine several parameters that can, possibly, play an important role in the interaction between solar wind dynamic pressure pulses and the magnetosphere. The most natural parameter to be considered is obviously the solar wind dynamic pressure itself (P_{dyn}). Previous studies mentioned in section 1 above *[Meurant et al., 2003, 2004]* have however shown that this may not be the most important parameter. We will nevertheless consider this parameter, as well as its variation (maximum value, pressure jump, rate of change etc) for correlation with the magnetospheric response expressed in terms of open flux, closure voltage etc. The second natural parameter is the solar wind velocity (v_{sw}), that has already been pointed out as a key parameter governing the magnetospheric response to a solar wind pressure pulse. The solar wind density (n_{sw}) is also considered, but these three solar wind properties are not independent, as $P_{dyn} = n_{sw}\, m\, v_{sw}^2$. The interplanetary magnetic field (IMF : B_{sw}) has also to be studied, not only its magnitude, but also the value of each component, and their variations. The solar wind properties can be combined according to the model of *Petrinec and Russell* [1993, 1996], to estimate the size of the magnetospheric cavity: the "radius" of the magnetopause R_M (i.e. the distance between the dayside nose of the magnetopause and the planet), the radius at $x_{GSM} = 0$ and its cross section may be important, as well as the variations of these quantities. The standoff distance of the bow shock R_B can also be treated in a similar manner.

We also consider the magnetospheric response in terms of its signature at geosynchronous altitude. More specifically, the elevation angle of the magnetic field is studied on the nightside using data from the GOES-8 satellite. These data are available only for a subset of events, so that less accurate results may be obtained.

We anticipate the next sections by summarizing in **Table 1** the quantities that will be actually discussed in this paper and their definition. In this study, the time interval reported in **Table 1** is that of the pressure pulse-induced flux closure. More variables and correlation pairs were considered initially, but we will focus on the ones we found to be the most interesting. Several variables specifically deal with the ramp of the dynamic pressure front. The front ramp is determined as follows: the time derivative of the solar wind pressure is computed using a Savitzky-Golay filtering [*Savitzky and Golay, 1964*], and the time interval of increasing dynamic pressure around the time of maximum derivative is considered as the ramp of the pressure front. This concept is however a bit loosely defined in the case of a very weak pressure pulse. The Savitzky-Golay smoothing filter can be used to smooth a noisy signal. The filter is defined as a weighted moving average with weighting given as a polynomial of a certain degree. The returned coefficients, when applied to a signal, perform a polynomial least-squares fit within the filter window. This polynomial is designed to preserve higher moments within the data and reduce the bias introduced by the filter, and the derivatives of the smoothed signal can be obtained.

3. Statistical Analysis

The variables discussed in Section 2 have been searched for correlation. A set of 68 solar wind dynamic pressure pulse events has been identified in the SI12, SuperDARN and ACE datasets, and treated to estimate the open flux, reconnection voltages, dynamic pressure etc of these intervals. The method outlined above is applied to determine the duration of each pulse interval. Correlations are searched for between the geomagnetic quantities (open flux, voltages, elevation angle etc, and their variations) and solar wind properties. The correlation is studied using both Fisher's test and the Student test. The significance level of the correlations are obtain in the sense of bilateral tests, and the critical level of confidence is such that the estimated Pearson correlation coefficient equals one of the limit of the test interval that brackets correlation cases undistinguishable from the case r = 0. For the student test, the quantity $\frac{\hat{r}\sqrt{n-2}}{\sqrt{1-\hat{r}^2}}$ ($\hat{r}$ being the estimated correlation coefficient) is known to follow a t_{n-2} distribution function under the $r = 0$ hypothesis, which allows bilateral testing. In the case of the Fisher test, the quantity $z = \frac{1}{2}\ln\left(\frac{1+\hat{r}}{1-\hat{r}}\right)$ is calculated, which is known to follow a Gaussian distribution $N\left(\frac{1}{2}\ln\left(\frac{1+r}{1-r}\right), \frac{1}{\sqrt{n-3}}\right)$ which again allows us to perform a bilateral testing under the $r = 0$ hypothesis. Whatever the test used, the (critical) level of confidence tells us how confident we should feel that the estimated correlation coefficient differs from zero, whereas the square of the correlation coefficient (also called the coefficient of determination) tells us what fraction of the variance of the dataset could be explained by the dependence of both data on each other. From a mathematical standpoint, the Fisher test is known to be inefficient for small size samples (less than ~25 data pairs), whereas the Student test is always valid. Clearly, both tests give different significance levels for a given sample, but both significance levels tend to the same limit as the sample size is increased. Obviously, if n tends to infinity, one is supposed to reach absolute certainty and the significance level is always 1, whatever the test used. (In the following paragraphs, we will use the symbol r instead of $\hat{r}$.) In our study, both tests give very similar results. More than 1200 pairs of variables were considered. A very large number of these pairs were found to be (linearly) correlated under a level of confidence of 0.9. Clearly, much higher levels of confidence must be used to identify the correlation. The critical level of confidence was determined for each pair of variables (i.e., the level of confidence under which the correlation coefficient of the considered pair of variables is equal to the threshold value that discriminates between correlated and uncorrelated variables, i.e. between non-zero and zero correlation coefficient). From a mathematical standpoint, it is impossible to define an absolute threshold that discriminates once and for all between correlated and uncorrelated samples of paired variables. Only a hypothesis test can be carried out and the significance of a correlation must be expressed in terms of a level of confidence. The significance is however not the final word, as a low correlation can be statistically significant, and the square of the correlation coefficient can be used as a measure of the part of the variations in the dataset that can be explained by the dependence between the correlated variables. In this study, we will essentially present the most significant correlations. The critical level of confidence can be estimated according to Fisher's or Student's test. We will always quote the worst of these two. For every variable, outliers are systematically eliminated: data points such that $|x_i - m| > 3\sigma$ are rejected, with m the average value of the ensemble $\{x_i\}$, and σ the standard deviation of the sample. One can consider that this is a rather conservative choice that tends to reduce the inferred correlations, because in a collection of sets of 68 data points, an average of ~0.18 points per sample would fall outside of the $|x_i - m| > 3\sigma$ interval, assuming a Gaussian distribution of the data, so that one can expect that a data point representative of the natural distribution may be found outside of the selected interval in ~20% of the cases.

Figure 2 shows the distribution function of several properties of the solar wind for our set of events. The dotted lines show the distribution function and a smoothing is applied to produce the solid lines. The average (m) and standard deviation (σ) of the sample are also given. The bin size used to construct a distribution function is $10 \times \sigma/\tilde{n}$ with $\tilde{n}$ the number of points of the sample found in a 2σ- wide interval centred on m. The dynamic pressure increase across the pressure front is shown in the top panel. It clearly appears that most of the fronts included in this study were rather weak: the median of the distribution is 3 nPa. This also appears in the solar wind density increase across the pressure pulse (middle panel) with a median value of 9.15 cm^{-3} and a most probable value of ~4 cm^{-3}. The variation of the solar wind speed across the dynamic pressure discontinuity (third panel) is generally positive, although the most probable value is ~0 km/s. Indeed, as the dynamic pressure is proportional to the square of the velocity, a small increase of the velocity will produce a large increase of the dynamic pressure (a 10% increase of the velocity produces a 20% increase of the dynamic pressure).

Considering the net open flux budget, the value of the open flux at the end of the pressure pulse-induced flux closure (Φ_{final}) is, first of all, correlated with the open flux available prior to the pressure front arrival (Φ_{init}) (**Figure 3, Table 2**). The correlation coefficient is $r = 0.807$, and the correlation hypothesis must be accepted with a confidence level better than $\alpha = 0.999$ (according to both Fisher and Student tests). (Throughout this paper, we will denote a correlation coefficient with the symbol r, and a level of confidence with the symbol α.) This correlation can account for $r^2 = 0.65$ (65%) of the observed variance, so that much larger correlations must not be expected with other parameters, and Φ_{init} is considered here as one of the independent variables. Indeed, the value of Φ_{init} results from the past history of the solar wind – magnetosphere interaction and represents a preconditioning of the system. As may be expected, the final open flux also correlates with the IMF B_z. The Φ_{final} and $B_{z,\text{max}}$ (generally positive) are anticorrelated (accounting for ~17% of the variance only) (**Table 2**). This can be easily understood: when the IMF is northward, very little open flux can be created on the dayside, and the open flux is then lower. The relation between the IMF B_z component and the creation of open flux is already well known, so we will not dwell on this subject. The final amount of open flux also anticorrelates with the maximum value of P_{dyn}, $P_{dyn,max}$ and with the pressure jump (ΔP_{dyn}). Strong compression of the tail thus favours lower values of Φ_{final} , but the amount of open flux itself depends more on the past history of the magnetosphere through Φ_{init} , both correlations with $P_{dyn,max}$ and ΔP_{dyn} being able to account for ~9% of the variance only.

The variation of the open flux ($\Delta\Phi$), which results from the balance between flux opening on the dayside and flux closure in the tail, and the amount of flux closed during the event (i.e. $\Phi_{cl} = \int_{t_0}^{t_1} V_{cl}\, dt$ with V_{cl} the closure voltage and $[t_0,t_1]$ the considered time interval) may be quantities much more representative of the magnetosphere – pressure front interaction rather than the amount of open flux itself. However, the best correlation for both quantities is found with Φ_{init} as well (**Figure 4, Table 3**) explaining 16-17% of the variance. Indeed, $\Delta\Phi = \Phi_{final} - \Phi_{init}$ and Φ_{final} already correlates with Φ_{init} . Also, Φ_{cl} represents the amount of open flux that goes through reconnection and, if the amount of open flux newly created on the dayside during the considered interval is not too large, Φ_{cl} cannot be larger than Φ_{init}. But this correlation nevertheless suggests that, as the magnetosphere accumulates open flux, its ability to close flux in the tail under the stimulation of a pressure pulse is increased ($\Delta\Phi$ and Φ_{cl} are negative numbers). The importance of magnetospheric preconditioning also appears in the correlation of $\Delta\Phi$ and Φ_{cl} with the maximum value of the magnetopause radius (the standoff distance of the magnetopause) $R_{M,max}$ computed based on solar wind data using the model of *Petrinec and Russell* [1993, 1996], both being able to explain ~10% of the variance. Similar correlations are also found with the standoff distance of the bow shock $R_{B,max}$ and with the initial values of R_M and R_B: $R_{M,init}$ and $R_{B,init}$, with slightly lower confidence.

These correlations suggest that the magnetospheric preconditioning is not limited to the accumulated open flux, but also includes the cross section of the magnetospheric cavity exposed to the solar wind flow, the standoff distance being considered here as a rough proxy describing the shape of the magnetosphere. In the model of *Petrinec and Russell* [1993, 1996], the standoff distance of the magnetopause is a complicated non-linear function of both B_z and P_{dyn}, and one may wonder if the correlation with the magnetopause radius does not stem from a correlation with P_{dyn}, especially with its initial value, or with its variation across the dynamic pressure front. In our sample, which includes weak pulses, we found that the dynamic pressure does not seem to strongly drive the flux closure process, as we will show below. It can also be noted that Φ_{op}, the amount of open flux created on the dayside during the pressure pulse-induced flux closure interval, and Φ_{cl} do not well correlate with each other (***Table 3***), suggesting that tail reconnection closes accumulated open flux rather than newly opened flux. Neither is a significant correlation found between Φ_{op} and $\Delta\Phi$. This supports the importance of the loading-unloading paradigm, in which open magnetic flux and energy are accumulated in the tail before intense flux closure can begin, compared with the direct driving of the magnetosphere by the solar wind [*Blockx et al., 2009,* and references therein] in which new magnetic energy is supplied through the tail magnetopause and is nearly immediately available for dissipative processes. Indeed, the transport of magnetic flux from the dayside magnetopause to the nightside reconnection site can take of the order of one hour. It is no surprise, however, that Φ_{op} is well correlated with $B_{z,min}$ (r = -0.437, α = 0.999) as a southward IMF (i.e. a negative IMF B_z) is a condition that strongly stimulates magnetic reconnection on the dayside.

The value of the flux closure voltage itself basically correlates with Φ_{init} (**Figure 5, Table 4**): the average reconnection voltage $\overline{V_{cl}}$ has its best correlation with Φ_{init} (r^2 *~ 21%).* $\overline{V_{cl}}$ then correlates with $R_{M,max}$ and $R_{B,max}$ (r^2 ~ 17%). The median voltage computed during the considered time interval, $\underline{V_{cl}}$, has its best correlation with Φ_{init}, then with $R_{M,max}$ and $R_{B,max}$ possibly representing ~16-17% of the variance. (Note that $R_{M,max}$ and $R_{B,max}$ are not independent on each other). Slightly lower correlations are again found with $R_{M,init}$ and $R_{B,init}$ (**Figure 5, Table 4**). These correlations show that the preconditioning of the magnetosphere is important for the process of flux closure itself. These results do not really differ from those presented for Φ_{cl}, as in principle, $\Phi_{cl} = \overline{V_{cl}}\,\Delta t$, with Δt the duration of the pressure pulse-induced flux closure interval. (Note that, in our study, Φ_{cl} is not exactly equal to $\overline{V_{cl}}\,\Delta t$ because Φ_{cl} is obtained from a numerical integration, whereas $\overline{V_{cl}}$ is the simple arithmetic average of the discrete series of closure voltage values. This choice was made to ease the comparison between $\overline{V_{cl}}$ and $\underline{V_{cl}}$, whereas Φ_{cl} has to be compared with $\Delta\Phi$.)

The minimum value reached by the closure voltage $V_{cl,min}$ represents the maximum rate of flux closure, because V_{cl} is a negative number. This quantity best correlates with $R_{M,max}$ and $R_{B,max}$ (r^2 ~ 17%) (**Table 5**). Similar correlations are found with $R_{M,init}$ and $R_{B,init}$, which, naturally, are close to $R_{M,max}$ and $R_{B,max}$, respectively. Solar wind properties correlate slightly better with $V_{cl,min}$ than Φ_{init}. The variation of the IMF intensity $\Delta|B|$ correlates with $V_{cl,min}$ as well as its average rate of change during the dynamic pressure front ramp $\overline{\left.\frac{d|B|}{dt}\right|_{ramp}}$ and the variation of the solar wind velocity across the ramp of the pressure pulse $\left.\Delta v_{sw}\right|_{ramp}$. These last correlation coefficients remain weak. (All these correlations can account for 10-12% of the variance). The solar wind dynamic pressure does not seem to play a significant role so far in the analysis of the sample of dynamic pressure pulse-induced flux closure presented here (although the dynamic pressure and the solar wind velocity are dependant quantities).

The only potential-related parameter that we find to be well correlated with one of the solar wind properties is the intensification of the closure voltage $\Delta V_{cl} = V_{cl,max} - V_{cl,init}$, the difference between the maximum and initial closure voltage as determined on the basis of SI12 and SuperDARN observations. ΔV_{cl} correlates best with $\Delta|B|$ and with $\left.\Delta v_{sw}\right|_{ramp}$ (**Table 6**). These correlations can represent only ~9-12% of the observed variances. The level of confidence of these correlations is somewhat lower than the values presented above, that had levels of confidence reaching 0.999. An increase in the modulus of B, as well as an increase of the velocity implies an increase of the electric field of the solar wind, which is the cross product of the velocity and magnetic field (we exclude here the improbable situation in which the increase of B – v – would only take place along the component parallel to $\vec{v}$ – $\vec{B}$, respectively –). One can here wonder if a possible penetration of the interplanetary electric field into the magnetosphere can significantly influence the process of magnetic reconnection. This might be supported by the fact that the best correlation of ΔV_{cl} is found with Φ_{op} which, in principle, is proportional to the electric field in the solar wind, whereas we have seen above that the magnetosphere essentially closes a part of the accumulated open flux rather than the newly opened flux.

Inspection of the correlations found between the solar wind properties and the quantities representative of the closure process suggests that the pressure fronts of our dataset rather had the effect of initiating the flux closure process, which was controlled by the properties of the magnetosphere. Indeed, the flux closure is not strongly correlated with the pressure jump. To a first approximation it does not depend on the properties of the solar wind pressure front, but rather on the initial state of the magnetosphere. Clearly, if independent parameters had to be selected as the main variables that control the compression-induced flux closure process, one could select Φ_{init} and $R_{M,max}$ in the first place, possibly supplemented by $\Delta|B|$ and $\Delta v_{sw}\big|_{ramp}$ The dynamic pressure discontinuity is rather presented here as a trigger that favours the growth of some instability of the magnetosphere and, more specifically, of the plasma sheet, that eventually ends in a relaxation of the whole system through flux closure, that reconfigures the field of the magnetotail. **Figure 6** shows the lack of correlation (**Table 7**) between the dynamic pressure increase ΔP_{dyn} and the closure voltage intensification ΔV_{cl} (**Figure 6a**) and the closed flux Φ_{cl} (**Figure 6b**). The dispersion of the full dataset is such that no significant correlation can be found. However, **Figure 6a** also suggests that a subset could be isolated for ΔP_{dyn} > ~2.8 nPa (the method used to determine this threshold is explained in the next section: it corresponds to an optimal correlation). The dotted vertical lines in **Figure 6a,b** isolate this subset, and the solid lines are the least absolute deviation fits through the data. For the subset, higher correlation coefficients are found for ΔV_{cl} and Φ_{cl} with ΔP_{dyn} (**Table 7**), representing nearly 25% of the variance. This suggests on statistical grounds that a sufficiently strong solar wind dynamic pressure pulse can directly influence the flux closure process. Indeed, a previous study of *Hubert et al.* [2006b] showed that a strong compression of the tail can actively stimulate the flux closure process in the plasma sheet. Considering the distribution function of ΔP_{dyn} in **Figure 2**, it clearly appears that most of the pressure fronts included in our dataset were weak ones, and one could wonder if weak and strong pressure pulses have the same impact on the magnetosphere. Indeed, it may seem surprising that the defining parameter of an interplanetary pressure front does not influence at all the response of the magnetosphere to a pressure pulse.

4. Subset Statistics

As the properties of the solar wind pressure fronts in our dataset do not appear to significantly influence the magnetospheric response expressed in terms of flux closure, we conducted an analysis aimed at identifying subsets in the dataset for which a better correlation is found between the flux closure-related parameters and the solar wind-related parameters. The quality of the correlation is not determined by the value of the correlation coefficient itself, but rather by the level of confidence in the correlation, which combines the correlation coefficient and the number of observations available in the (sub)sample. Outliers are rejected from the analysis by applying the same procedure to the subset of data as that described above for the full dataset.

It has been possible to find thresholds on various dynamic pressure-related parameters that isolate subsets of events for which a correlation is found with the variables describing the response of the magnetosphere in terms of flux closure. We propose to use these thresholds to quantify what can be considered as a strong solar wind dynamic pressure pulse, i.e. a pulse that causes a magnetospheric response sensitive to the dynamic pressure itself. All things considered, identifying dynamic pressure fronts implicitly assumes that dynamic pressure variations can be classified into two categories: modest variations on the one hand, and pulses on the other, without proposing a well defined criterion allowing us to discriminate between them. In our dataset selection, we chose to classify dynamic pressure variations as fronts if they produce a dayside subauroral proton flash, to be detected in the SI12 images. This criterion makes sense because the dayside subauroral proton flash is a natural signature indicating a sudden compression of the dayside magnetosphere by the solar wind. Nothing guarantees, however, that this dayside-based criterion allows us to fully appreciate the nature of a dynamic pressure variation in terms of the nightside response of the magnetosphere to a dynamic pressure front.

Pressure fronts presenting a solar wind dynamic pressure increase ΔP_{dyn} larger than ~2.8 nPa form a subset for which ΔP_{dyn} and ΔV_{cl} correlate well, so that their interdependence could account for ~25% of the variance of the subsample (**Figure 7, Table 8**). This clearly expresses a reaction of the magnetosphere in response to the dynamic pressure increase in terms of an intensification of the flux closure rate. The same threshold value of ~2.8 nPa was found when searching for the best possible correlation between ΔP_{dyn} and $V_{cl,min}$ but the correlation coefficient was found to be rather low, as well as the level of confidence. Finding the same threshold for these two parameters is not surprising, as they are not independent of each other. It nevertheless suggest that, for strong pressure fronts, the solar wind dynamic pressure partly controls the process of flux closure in the tail by compressing it, as explained in *Hubert et al.* [2006b]. Variable Φ_{cl} is found to have a better correlation with ΔP_{dyn} for a threshold of ~2.8 nPa as well, the correlation accounting for ~12% of the variance, while $\underline{V_{cl}}$ and $\overline{V_{cl}}$ are both found to better correlate with ΔP_{dyn} for a threshold of ~3 nPa. The threshold for correlation with $\Delta\Phi$ is 2.8 nPa as well, but the correlation coefficient is very low. A reasonable threshold to discriminate between strong and weak pressure pulses based on the dynamic pressure increase across the dynamic pressure jump could therefore be chosen as ~2.8 – 3 nPa. This value of the pressure increase can be compared with the typical value of the solar wind dynamic pressure, i.e. 3 nPa [*Feldman, 1977*]. Not surprisingly, a threshold could also be found for the maximum rate of change of the dynamic pressure $\left.\frac{dP_{dyn}}{dt}\right|_{\max}$ (**Table 9**). A maximum level of confidence on correlation is found for this parameter with ΔV_{cl} (r^2 ~ 34%), Φ_{cl} (r^2 ~ 24%), $\overline{V_{cl}}$ (r^2 ~ 14%) and $V_{cl,min}$ (r^2 ~ 22%) for a threshold value of $\left.\frac{dP_{dyn}}{dt}\right|_{\max} > 2.14\times10^{-2}$ nPa/s, whereas a threshold of 1.80×10^{-2} nPa/s gives a maximum level of confidence for correlation with $\underline{V_{cl}}$ (r^2 ~ 12%) and $\Delta\Phi$ (r^2 ~ 6%, this value being rather low). A typical threshold could be chosen based on these results, but the dynamic pressure growth has also to last for a sufficiently long time to produce a significant pressure increase.

The closure voltage intensification ΔV_{cl} and the total amount of flux closed Φ_{cl} are also found to be well correlated with the maximum dynamic pressure reached during the pressure pulse-induced flux closure interval P_{max} (**Figure 8, Table 10**), restricting the dataset to events with $P_{max} > 5.97$ nPa (r^2 ~ 28%; r^2 ~ 11% respectively). Maximum levels of confidence on correlation are found between P_{max} and $V_{cl,min}$, $\underline{V_{cl}}$ and $\overline{V_{cl}}$ when restricting to $P_{max} > 6.14$ nPa, with poorer correlation however (r^2 ~ 12%; r^2 ~ 7%; r^2 ~ 7% respectively). A reasonable threshold for a strong pressure pulse could thus be chosen as $P_{max} > 6$ nPa, but the net change of dynamic pressure must nevertheless be considered as well, as shown above, because the solar wind can present intervals of steady high dynamic pressure. Indeed, the dependence on P_{max} is not able to account for much of the variance of the studied subsets.

Variations of the solar wind velocity are not only associated with variations of the electric field in the solar wind, they are also able to produce strong variations of the dynamic pressure. Both effects could influence the process of magnetic flux closure in the tail. Indeed, ΔV_{cl} and $\left.\Delta v_{sw}\right|_{ramp}$, the variation of the solar wind velocity during the ramp of the dynamic pressure front, are strongly correlated (r^2 ~ 34%) = -0.586, $\alpha = 0.9997$) if the analysis is restricted to events with $\left.\Delta v_{sw}\right|_{ramp} > 11.3$ km/s (**Figure 9, Table 11**). The correlation is even better with the other variables related with the closure voltage, the correlation being able to account for 53% of the variance of $\underline{V_{cl}}$. It clearly appears that an increase of the solar wind velocity by more than 11-12 km/s during the ramp of the dynamic pressure front causes a stronger response of the magnetosphere in terms of flux closure.

Very similar results are obtained concerning the variation of the solar wind velocity across the whole interval considered ($\Delta v_{sw} = v_{sw,max} - v_{sw,init}$), but with a threshold value of ~8.6 km/s, i.e. roughly 25% lower than the threshold obtained for $\Delta v_{sw}\big|_{ramp}$ (**Table 12**). This difference could however be due to the fact that $\Delta v_{sw} \geq \Delta v_{sw}\big|_{ramp}$, which can slightly modify the correlations. As this threshold is independent of the manner in which the ramp is defined, it may finally be a more suitable threshold. One could argue that a 12 km/s increase in the solar wind velocity can take place progressively during a long interval, and should not be considered a pulse. Indeed, we could also identify threshold values for the maximum rate of change of the solar wind velocity. All thresholds found were larger than 0.22 km/s^2. A more typical value could be ~0.286 km/s^2 (**Table 13**).

Considering the full dataset, it has been found above that a variation of the IMF intensity influences the flux closure process in the tail, from a statistical standpoint. Keeping the subset of events for which $\Delta|B| > 0.47$ nT (**Table 14**), one finds much better correlations for ΔV_{cl}, $V_{cl,min}$, Φ_{cl}, $\overline{V_{cl}}$ and $\underline{V_{cl}}$. Indeed, this nearly zero threshold value suggests that, in fact, an increase of the IMF magnitude favours the process of dynamic pressure pulse-induced flux closure. Further studies should elucidate if this is specific to the pulse-induced flux closure, or if this is a general trend including flux closure intervals unrelated to a dynamic pressure front.

The last paragraphs indicate that strong solar wind dynamic pressure pulses can be defined, from the standpoint of their implication on the process of flux closure, as pressure fronts presenting the following characteristics: a dynamic pressure increase of ~3 nPa, and/or a dynamic pressure reaching ~6 nPa, and/or a velocity increase by some ~10 km/s. Events combining these three properties should naturally be expected to be very efficient at directly stimulating flux closure in the magnetotail. In addition, an increase of the IMF magnitude is also a factor that favours a more intense closure voltage, but this is not necessarily specific to pressure pulse-induced flux closure intervals and should be checked by further studies.

The predominant importance of variations of the solar wind velocity can be highlighted by a full analysis of the subset defined by ΔP_{dyn} > 2.8 nPa. For this subset, the variation of the solar wind velocity is found to be the one that best correlates with ΔV_{cl}, $V_{cl,min}$, Φ_{cl}, $\overline{V_{cl}}$ and $\underline{V_{cl}}$ (**Table 15, Figure 10**), the correlations explaining between 30 and 46% of the variations. The correlation between the variation of the solar wind velocity and the parameters describing the pressure pulse-induced flux closure is obvious. It must be noted that the preconditioning by the accumulated open flux prior to the pulse arrival at Earth plays now a minor role. Indeed, Φ_{init} correlates with Φ_{cl} with r = -0.318 and α = 0.955 only. All other correlations between Φ_{init} and the variables listed here are poorer. Clearly, a small correlation remains, especially with Φ_{cl}, because the amount of available open flux limits the amount of flux that can go through closure, but for strong pressure pulses, this remains a minor factor compared with the solar wind properties. It must be noted that ΔP_{dyn} correlates significantly with ΔV_{cl} (r = -0.483, α~0.997), whereas no other voltage-related parameter correlates well with ΔP_{dyn}. This suggests that, for strong pressure fronts, the compression of the magnetosphere leads to an intensification of magnetic reconnection without determining the value of the reconnection rate itself. The other voltage-related parameters better correlate with parameters related with the solar wind velocity: Δv_{sw}, as explained above but also $\left.\Delta v_{sw}\right|_{ramp}$, $\left.\frac{dv_{sw}}{dt}\right|_{max}$ etc. Another parameter that appears in the correlation analysis is the radius of the magnetopause at $x_{GSM} = 0$, i.e. at Earth location ($\Delta R_{M\text{-}E}$, not listed in table 1). Its associated correlation coefficients, ranging between 0.45 and 0.56, are generally lower than those found for the velocity-related parameters. The magnetospheric radius can be found at any x_{GSM} using a proxy based on the solar wind properties [*Petrinec and Russell, 1993, 1996*] and is dependant on the solar wind velocity, the interplanetary magnetic field etc. $\Delta R_{M\text{-}E}$ can be viewed as a proxy for the compression of the magnetosphere that only depends on the solar wind properties, and these correlations show again the compression of the tail favours flux closure. If a set of independent variables that contribute to determine the magnetospheric response to strong solar wind dynamic pressure discontinuities had to be selected, one could probably choose Δv_{sw} and ΔP_{dyn} in the first place, possibly supplemented by $\Delta R_{M\text{-}E}$, but it would not be necessary to include the magnetospheric preconditioning, in contrast with the results found for the full dataset.

5. Correlations with Geosynchronous Data

For a restricted subset of events, the GOES-8 satellite was located in the midnight sector, which we consider here as a 6 h MLT interval centred on midnight MLT. We obtained 24 events satisfying that requirement. The elevation angle of the magnetic field measured at geosynchronous altitude by the GOES-8 satellite, as well as its variations, was compared with the results obtained from the SI12 and SuperDARN data to describe the open flux and the closure voltage.

The open flux Φ_{init} accumulated prior to the solar wind dynamic pressure front arrival is correlated with the initial (prior to the front arrival) value of the elevation angle e_{init} (r = -0.762, α = 0.998, **Figure 11**). This is not surprising, considering that both quantities describe two different aspects of the state of the magnetosphere, which as a whole results mainly from its past interaction with the solar wind. The open flux accumulated by the magnetosphere can be seen as the set of flux tubes that originate in the ionosphere and close though the interplanetary medium. The accumulation and variation of the open flux results from the imbalance at “short” time scales (typically ~an hour, i.e. the time scale of the substorm cycle) between the flux opening on the dayside and flux closure in the tail. As the magnetosphere is accumulating open flux, open flux tubes are dragged downtail by the motion of the solar wind, which eventually produces a stretching of the tail, until open flux gets closed by magnetic reconnection reducing both the stretching (return flow of the flux tubes) and the amount of open flux. Both quantities, open flux and tail stretching expressed here in terms of geosynchronous elevation angle, thus evolve in a dependant manner and will, to some extent, be correlated. The natural consequence is that we should expect the flux closure process and the elevation angle to be partly related to each other.

The minimum value of the closure voltage $V_{cl,min}$ which represents the extreme rate of flux closure, is correlated with the minimum rate of change of the geosynchronous elevation angle $\left.\frac{de}{dt}\right|_{min}$ (r = 0.510, α = 0.992 –Fisher test-; α = 0.985 –Student test- , **Figure 12**). A reduction of the elevation angle is the signature of a change of the geomagnetic field to a less dipolar configuration, so that its rate of change during a flux closure interval can be expected to be positive. On the other hand, the compression of the tail by the solar wind dynamic pressure pulse can be expected to produce a less dipolar configuration by moving the tail plasma towards the plasma sheet, together with the frozen-in magnetic field lines that it hosts, thus producing a decrease of the elevation angle. From that standpoint, $\left.\frac{de}{dt}\right|_{\min}$ can be seen as a proxy for the extreme rate of change of the magnetic field towards a compressed, less dipolar, configuration. We thus find that the extreme rate of flux closure is correlated with a proxy that, in the case of the interaction of the magnetosphere with a dynamic pressure front in the solar wind, describes the extreme rate of compression of the tail. The correlation that we find suggests that a sharper compression of the tail leads to a stronger extreme rate of flux closure. However, ΔV_{cl} and the variation of the elevation angle during the ramp of the solar wind dynamic pressure front Δe_{ramp} are negatively correlated (r = -0.453, α = 0.981 -Fisher test-; α = 0.970 –Student test- , **Figure 11**), showing that on a slightly longer time scale, the closure voltage intensification dominates the dynamics of the magnetospheric topology and configuration, driving it towards a more dipolar shape. It follows that, in the case of strong solar wind dynamic pressure pulses, the direct compression of the tail (expressed in terms of the extreme rate of decrease of the elevation angle) causes a transient stimulation of the flux closure: the stronger the compression, the stronger the extreme value of the closure rate, but it must be stressed that the negative value of $\left.\frac{de}{dt}\right|_{\min}$, which is a value obtained punctually at a given time of the pressure front interval, does not preclude the geomagnetic field from undergoing a global dipolarization on longer time scales during that interval. Nor does this result preclude other parameters from influencing the closure process, but it stands along the same lines as the results from *Hubert et al.* [2006b] who also showed that a pressure front can drive transient flux closure by direct compression of the magnetotail down to the plasma sheet. The first consequence of a compression of the tail is an increase of the current density within the plasmasheet. If we note L the characteristic scale of the magnetospheric cavity, which is reduced by the compression, then the conservation of magnetic flux during the compression implies that the magnetic field strength (B) increases proportionally to $\sim 1/L^2$. In addition, the width of the plasma sheet (w) can be expect to decrease proportionnaly to $\sim L^{1.4}$ (approximately, for an adiabatic compression to match the field pressure in the lobes), so that the current density, which is roughly proportionnal to 2B/w, increases according to $\sim 1/L^{3.4}$. If the characteristic scale can be expected to vary roughly proportionnally to $P_{dyn}^{-1/6}$ [*Kivelson and Russell, 1997*], then the current density can be expected to vary proportionnally to $\sim P_{dyn}^{0.57}$, i.e. a bit faster than the square root of the dynamic pressure, so that it may reasonably be supposed that a sharp increase in the plasma sheet current density produced by a dynamic pressure increase could trigger an instability starting or simply increasing the reconnection rate. The velocity of the plasma flowing out of the reconnection site is, in a first approximation, the Alfvèn speed $V_A = B/(\mu_0 \rho)^{½}$, and under the frozen-in approximation, the electric field is, $E_y \sim B_z V_A$ [*Owen and Cowley*, 1987]. The effect of compression is to increase both the magnetic field and the plasma density. If in addition we assume that the field and the density increase at roughly the same rate (i.e. a doubling of the field would take place along with a doubling of the plasma density), then we can expect that V_A will also be increased by the compression (for example, a doubling of both B and ρ increases V_A by a factor ~1.41). We do not expect that B_z would be much increased by the compression because, in a slightly idealized view of the magnetotail, the magnetic effect of compression is to move field lines roughly parallel to the plasma sheet closer to each other, modifying the magnetic flux threading a surface element perpendicular to the sheet. It follows that the newly closed field lines are efficiently evacuated from the reconnection site due to higher V_A. It also follows that a larger electric field can be expected in the vicinity of the reconnection site when the plasma sheet is compressed, consistently with the increase of the Alfvèn speed that results from the competing increase of both the plasma density and magnetic field, suggesting an increased reconnection rate. In addition, one could also speculate that a stronger compression of the tail could lead to the formation of a reconnection site of larger extent favouring a larger value of the extreme rate of flux closure.

6. Discussion

A statistical study, and especially a statistical correlation study, must be analyzed considering the possible physical mechanisms that lead to a correlation between two parameters. Two quantities can be found to be correlated despite the lack of causal relation between them. Moreover, for large data samples, statistical tests very often indicate the presence of a correlation between variables that are obviously unrelated on physical grounds. In the present study, a very large number of parameters were defined and correlated with each other. We restricted our manuscript to the most significant and physically meaningful correlations. Proceeding this way, we may have excluded correlations between parameters that are truly related on physical grounds but for which the scatter of the dataset does not allow us to identify a strong correlation. On the other hand, the most significant correlations that we presented very likely rely on physical processes.

In our search for a criterion allowing discriminating between strong and weak solar wind dynamic pressure pulses, several criteria were proposed. This could appear to be an inconsistency, because one would expect to find a single criterion. However, the concept of a strong dynamic pressure pulse is somewhat imprecise, and the complexity of the coupled solar wind – magnetosphere system is such that the response of the magnetosphere cannot be fully determined by a single parameter. It is thus not unacceptable to consider that strong pressure pulses can be defined according to several criteria that will not necessarily be simultaneously fulfilled. Indeed, as we already mentioned above, our identification of dynamic pressure pulses based on the excitation of a dayside subauroral proton flash also selects intervals with a rather weak dynamic pressure variation that does not much compress the tail and can be considered simply as a trigger that switches on the process of relaxation of the loaded magnetosphere. For these cases, it is not surprising to find that the flux closure process mostly correlates with parameters representing the initial state of the magnetosphere, i.e. its preconditioning. For stronger dynamic pressure pulses, the preconditioning of the magnetosphere still plays a role, but the properties of the dynamic pressure front are of importance as well.

Initially the most natural criterion for identification of strong dynamic pressure pulses is certainly that based on the dynamic pressure increase. However, the time scale in which the dynamic pressure increase takes place is also important. In this study, this aspect did not have to be explicitly considered because solar wind dynamic pressure pulses were identified based on a pragmatic observational criterion: we searched for dayside subauroral proton flashes to identify pulses. Consequently, the time scale limitation was implicitly included in the process of events selection: every selected interval did include a dynamic pressure variation that caused a rapid compression of the dayside magnetosphere, and could thus be considered as a dynamic pressure front, i.e. presenting a rapid variation of the pressure exerted by the solar wind on the magnetosphere. The dynamic pressure variation that we determined for our set of intervals thus always did take place on a sufficiently short time scale for the purpose of this study. A typical time scale can nevertheless be roughly estimated using the criterion based on the maximum rate of change of the solar wind dynamic pressure. We found strong pulse criteria to be $\Delta P_{dyn} > 2.8$ nPa, and $\left.\frac{dP_{dyn}}{dt}\right|_{\max} > 2.14\times10^{-2}$ nPa/s. The ratio of these two thresholds is 131 s. The typical time scale on which the dynamic pressure increase must take place is thus of the order of a few minutes.

The results obtained here on statistical grounds are in good agreement with previous studies. Clearly we find that flux closure takes place in response to the interaction between the magnetosphere and solar wind dynamic pressure fronts, as in previous studies by *Boudouridis et al.* [2003, 2004]. Although the auroral precipitation and flux closure are two different signatures of that interaction, we find, along the same lines as *Meurant et al.* [2004], that weak pressure pulses play only a triggering role on magnetic flux closure, in such a manner that the detailed properties of the solar wind pressure front have a minor influence on the magnetospheric response, compared with the influence of the initial state of the magnetosphere. However, we find that, in the case of a strong pressure pulse, the pulse does not only trigger the reconnection process in the tail, but also the solar wind properties significantly influence the magnetospheric response expressed in terms of flux closure, in contrast with *Meurant et al.* [2004]. We also find that a change of the IMF magnitude is an important parameter for dynamic pressure pulse-induced flux closure, especially for the intensification of the flux closure rate. For strong pulses, the solar wind velocity, and especially its variation, significantly influences the process of dynamic pressure pulse-induced flux closure, which recalls the results obtained by *Meurant et al.* [2004] concerning the auroral precipitation. On the effect of the preconditioning, we find that the amount of open flux available for closure prior to the arrival of a solar wind pressure front is a key parameter in the case of a weak pulse, along the same line as the results previously found by *Meurant et al.* [2004] for the B_z IMF component. In addition, we find that the size of the magnetospheric cavity also plays a preconditioning role in the case of a weak pressure pulse.

7. Conclusions

We conducted a statistical study of the flux closure in the tail related to solar wind dynamic pressure fronts. We found that the response of the magnetotail (in terms of flux closure) to a solar wind dynamic pressure front is mainly governed by the preconditioning of the magnetosphere in the case of weak pressure pulses ($\Delta P_{dyn} < 2.8$ nPa) whereas the properties of the solar wind become key parameters in the case of strong pulses ($\Delta P_{dyn} > 2.8$ nPa, taking place at the time scale of a few minutes). Indeed, strong pulses are capable of significantly compressing the geomagnetic tail, which vigorously stimulates magnetic reconnection in the plasma sheet. Geosynchronous data also show that the compression of the tail stimulates flux closure. In the case of a weak pulse, the preconditioning of the magnetosphere relies both on the amount of open flux accumulated prior to the arrival of the dynamic pressure front, and on the size of the magnetospheric cavity. In the case of a strong dynamic pressure pulse, the solar wind velocity, and especially its variation, is the solar wind property that influences the process of flux closure the most, although the variation of the solar wind dynamic pressure is also an important factor. The availability of open flux remains however a limiting factor. We also find that an intensification of the IMF favours the process of flux closure, but this may not be a specific feature of dynamic pressure pulse-induced flux closure intervals.

Acknowledgements The success of the IMAGE mission is a tribute to the many dedicated scientists and engineers that have worked and continue to work on the project. The PI for the mission is Dr J.L. Burch. Jean-Claude Gérard and Benoît Hubert are supported by the Belgian National Fund for Scientific Research (FNRS). This work was funded by the PRODEX program of the European Space Agency (ESA). Work at Leicester was supported by STFC grant PP/E000983/1. ACE level 2 data were provided by N.F. Ness (MFI) and D.J. McComas (SWEPAM), and the ACE Science Centre. GOES-8 data were obtained thanks to CDAWeb.

References

Blockx C., J.-C. Gérard, V. Coumans, B. Hubert, M. Meurant (2009), Contributions of the driven process and the loading-unloading process during substorms: A study based on the IMAGE-SI12 imager, J. Geophys. Res., 114, A02209, doi:10.1029/2008JA013280.

Boudouridis, A., E. Zesta, L. Lyons, P. Anderson, and D. Lummerzheim (2003), Effect of solar wind pressure pulses on the size and strength of the auroral oval, *J. Geophys. Res.*, 108(A4), CiteID 8012, doi:10.1029/2002JA009373.

Boudouridis, A., E. Zesta, L. R. Lyons, P. C. Anderson, and D. Lummerzheim (2004), Magnetospheric reconnection driven by solar wind pressure fronts, *Ann. Geophys.*, 22, 1367-1378.

Brittnacher, M., M. Wilber, M. Fillingim, D. Chua, G. Parks, J. Spann, and G. Germany (2000), Global auroral response to a solar wind pressure pulse, *Adv. Space Res.*, 25, 1377-1385.

Cowley, S.W.H. and M. Lockwood, Excitation and decay of solar wind-driven flows in the magnetosphere-ionosphere system (1992), *Ann. Geophys.*, 10, 103-115.

FeldmanW. C., J. R. Asbridge, S. J. Bame, and J. T. Gosling (1977), Plasma and magnetic fields from the sun, in The Solar Output and its Variation, edited by O. R. White, pp. 351-382, Colorado Associated University Press, Boulder.

Fuselier, S. A., , S. P. Gary, M. F. Thomsen, E. S. Claflin, B. Hubert, B. R. Sandel, and T. Immel (2004), Generation of Transient Dayside Sub-Auroral Proton Precipitation, *J. Geophys. Res.*, 109, A1227, doi:10.1029/2004JA010393.

Hubert, B., J.-C. Gérard, S. A. Fuselier, S. B. Mende (2003), Observation of dayside subauroral proton flashes with the IMAGE-FUV imagers, *Geophys. Res. Lett.*, 30, doi: 10.1029/2002GL016464.

Hubert, B., S. E. Milan, A. Grocott, C. Blockx, S. W. H. Cowley, and J.-C. Gérard (2006a), Dayside and nightside reconnection rates inferred from IMAGE FUV and Super Dual Auroral Radar Network data, *J. Geophys. Res.*, 111, A03217, doi:10.1029/2005JA011140.

Hubert B., M. Palmroth, T.V. Laitinen, P. Janhunen, S.E. Milan, A. Grocott, S.W.H. Cowley, T. Pulkkinen, and J.-C. Gérard (2006b), Compression of the Earth's magnetotail by interplanetary shocks directly drives transient magnetic flux closure, *Geophys. Res. Lett.*, 33, L10105, doi:10.1029/2006GL026008.

Kivelson, M. G. and C. T. Russell, Introduction to space physics, Cambridge University Press, Cambridge, UK, 1997.

Meurant, M.; J. C. Gérard; B. Hubert; V. Coumans; V. I. Shematovich; D. V. Bisikalo, D. S. Evans, G. R. Gladstone, S. B. Mende (2003), Characterization and dynamics of the auroral electron precipitation during substorms deduced from IMAGE-FUV, *J. Geophys. Res.*, 108, 1247, doi: 10.1029/2002JA009685.

Meurant, M.;J.-C. Gérard, B. Hubert, V. Coumans, C. Blockx, N. Østgaard, S. B. Mende (2003), Dynamics of global scale electron and proton precipitation induced by a solar wind pressure pulse, *Geophys. Res. Lett.*, 30, 2032 10.1029/2003GL018017.

Meurant, M., J.-C. Gérard, C. Blockx, B. Hubert, and V. Coumans (2004), Propagation of electron and proton shock-induced aurora and the role of the interplanetary magnetic field and solar wind, *J. Geophys. Res.*, 109, A10210, doi:10.1029/2004JA010453.

Mende, S.B., H. Heetderks, H.U. Frey, M. Lampton, S.P. Geller, S. Habraken, E. Renotte, C. Jamar, P. Rochus, J. Spann, S.A. Fuselier, J.C. Gérard, G.R. Gladstone, S. Murphree, and L. Cogger (2000a), Far ultraviolet imaging from the IMAGE spacecraft: 1. System design, *Space Sci. Rev.*, 91, 243-270.

Mende, S.B., H. Heetderks, H.U. Frey, J.M. Stock, M. Lampton, S. Geller, R. Abiad, O. Siegmund, S. Habraken, E. Renotte, C. Jamar, P. Rochus, J.C. Gérard, R. Sigler, and H. Lauche (2000b), Far ultraviolet imaging from the IMAGE spacecraft : 3. Spectral imaging of Lyman alpha and OI 135.6 nm, *Space Sci. Rev.*, 91, 287-318.

Owen, C. J., and S. W. H. Cowley (1987), Simple models of time-dependent reconnection in a collision-free plasma with an application to substorms in the geomagnetic tail, Planet. Space Sci., 35, 451-466.

Petrinec, S. M., and C. T. Russell (1993), An empirical model of the size and shape of the near-Earth magnetotail, *Geophys. Res. Lett.*, 20, 2695-2698.

Petrinec, S. M., and C. T. Russell (1996), Near-Earth magnetotail shape and size as determined from the magnetopause flaring angle, *J. Geophys. Res.*, 101, 137-152.

Ruohoniemi, J. M., and K.B. Baker (1998), Large scale imaging of high latitude convection with Super Dual Auroral Radar Network HF radar observations, *J. Geophys. Res.*, 103, 20797-20811.

Savitzky A. and M.J.E. Golay (1964), Smoothing and differentiation of data by simplified least squares procedures, *Anal. Chem.*, 36,1627-1639, doi: 10.1021/ac60214a047.

Tables

Symbol	Definition
n_{sw}	Solar wind numeric density
v_{sw}	Solar wind bulk velocity
$v_{sw,\ init}$	Initial value of v_{sw}, i.e. prior the the dynamic pressure pulse arrival
$v_{sw,\ max}$	Maximum value reached by v_{sw} after the dynamic pressure pulse arrival
Δv_{sw}	Variation of v_{sw} associated with the pressure pulse: $\Delta v_{sw} = v_{sw,\ max} - v_{sw,\ init}$
$\Delta v_{sw}\big\|_{ramp}$	Variation of v_{sw} over the ramp of the solar wind dynamic pressure pulse
P_{dyn}	Solar wind dynamic pressure
ΔP_{dyn}	Variation of P_{dyn} (pressure jump)
$P_{dyn\ max}$	Maximum value of P_{dyn} over a given time interval
$\left.\frac{dP_{dyn}}{dt}\right\|_{\max}$	Maximum value of the time derivative of P_{dyn} over a given time interval
$B_{z\ max(min)}$	Maximum (minimum, respectively) value of B_z over a given time interval
$\Delta\|B\|$	Variation of the IMF intensity over a given time interval
$\left.\frac{d\|B\|}{dt}\right\|_{ramp}$	Averga rate of change of the IMF intensity during the ramp of the solar wind dynamic pressure pulse
R_M	Radius of the magnetopause, i.e. standoff distance of the magnetopause
$R_{M,\ max}$	Maximum value of R_M over a given time interval
R_B	Radius of the bow shock, i.e. standoff distance of the bow shock
Φ	Open magnetic flux
Φ_{init}	Initial value of Φ prior to the solar wind dynamic pressure pulse arrival
Φ_{final}	Final value of Φ at the end of the pulse-induced flux closure interval
$\Delta\Phi$	$\Phi_{final} - \Phi_{init}$
V_{cl}	Magnetic flux closure voltage (a negative number)
$\overline{V_{cl}}$ *and* $\underline{V_{cl}}$	Average and median values (resp.) of V_{cl} over a given time interval.
$V_{cl,min}$	Minimum value of V_{cl} during a given time interval
$V_{cl,\ init}$	V_{cl} initial value, i.e. prior to the solar wind dynamic pressure pulse arrival
ΔV_{cl}	$V_{cl,min}$-$V_{cl,\ init}$: intensification of V_{cl} during the dynamic pressure pulse-induced flux closure interval.
Φ_{cl}	Amount of open flux closed during a given time interval. $\Phi_{cl} = \int_{t_0}^{t_1} V_{cl}\, dt$
V_{op}	Magnetic flux opening voltage
Φ_{op}	Amount of open flux created during a given time interval. $\Phi_{op} = \int_{t_0}^{t_1} V_{op}\, dt$
e	Elevation angle of the geomagnetic field at geosynchronous altitude from the GOES-8 measurements
e_{init}	Initial value of e, i.e. prior to the dynamic pressure pulse arrival
e_{min}	Minimum value of e over a given time interval
$\left.\frac{de}{dt}\right\|_{min}$	Minimum value of the time derivative of e over a given time interval
Δe_{ramp}	Variation of e during the ramp of the solar wind dynamic pressure pulse

Table 1. List of symbols used in this study.

Φ_{final}	r	α
Φ_{init}	0.807	>0.999
$B_{z\ max}$	-0.414	0.999
ΔP_{dyn}	-0.307	0.991
$P_{dyn,max}$	-0.298	0.988

Table 2. Correlation coefficients (r) and levels of confidence (α) for Φ_{final} with Φ_{init} , $B_{z\ max}$, ΔP_{dyn} , and $P_{dyn,max}$. α is the worst of the Fisher and the Student tests.

	Φ_{cl}		$\Delta\Phi$	
	r	α	r	α
Φ_{init}	-0.397	0.999	-0.410	0.999
$R_{M,max}$	-0.324	0.988	-0.332	0.990
Φ_{op}	-0.214	0.913	-0.06	0.612

Table 3. Correlation coefficients (r) and levels of confidence (α) for Φ_{cl} and $\Delta\Phi$ with Φ_{init} , $R_{M,max}$, and Φ_{op}. α is the worst of the Fisher and the Student tests.

	$\overline{V_{cl}}$		$\underline{V_{cl}}$	
	r	α	r	α
Φ_{init}	-0.456	> 0.999	-0.417	0.999
$R_{M,max}$	-0.410	0.999	-0.407	0.999
$R_{B,max}$	-0.408	0.999	-0.406	0.999

Table 4. Correlation coefficients (r) and levels of confidence (α) for $\overline{V_{cl}}$ and $\Delta\Phi$ with Φ_{init} , $R_{M,max}$, and $R_{B,max}$. α is the worst of the Fisher and the Student tests.

$V_{cl,min}$	r	α
Φ_{init}	-0.334	0.993
$R_{M,max}$	-0.415	0.999
$R_{B,max}$	-0.412	0.999
$\Delta\lvert B\rvert$	-0.335	0.993
$\overline{\left.\frac{d\lvert B\rvert}{dt}\right\rvert_{ramp}}$	-0.344	0.995
$\Delta v_{sw}\rvert_{ramp}$	-0.321	0.991

Table 5. Correlation coefficients (r) and levels of confidence (α) for $V_{cl,min}$ with Φ_{init} , $R_{M,max}$, $R_{B,max}$, $\Delta\lvert B\rvert$, $\overline{\left.\frac{d\lvert B\rvert}{dt}\right\rvert_{ramp}}$, and $\Delta v_{sw}\rvert_{ramp}$. α is the worst of the Fisher and the Student tests.

ΔV_{cl}	r	α
$\Delta\|B\|$	-0.352	0.996
$\Delta v_{sw}\|_{ramp}$	-0.300	0.985
Φ_{op}	-0.356	0.996

Table 6. Correlation coefficients (r) and levels of confidence (α) for ΔV_{cl} with $\Delta|B|$, $\Delta v_{sw}|_{ramp}$, and Φ_{op}. α is the worst of the Fisher and the Student tests.

ΔP_{dyn}		r	α
Full dataset	ΔV_{cl}	-0.166	0.827
	Φ_{cl}	-0.138	0.741
ΔP_{dyn} > ~2.8 nPa	ΔV_{cl}	-0.495	0.998
	Φ_{cl}	-0.490	0.987

Table 7. Correlation coefficients (r) and levels of confidence (α) for ΔP_{dyn} with ΔV_{cl} and Φ_{cl} for the full dataset (upper lines) and for the subset of data for which ΔP_{dyn} > ~2.8 nPa (lower lines). α is the worst of the Fisher and the Student tests.

ΔP_{dyn}	Threshold (nPa)	r	α
ΔV_{cl}	2.8	-0.495	0.9982
$V_{cl,min}$	2.8	-0.278	0.9045
Φ_{cl}	2.8	-0.340	0.9575
$\overline{V_{cl}}$	3	-0.220	0.7898
$\underline{V_{cl}}$	3	-0.283	0.8958
$\Delta\Phi$	2.8	-0.162	0.6752

Table 8. Subset thresholds and correlations for ΔP_{dyn}. The correlation coefficient r and level of confidence α of the Student test are obtained between ΔP_{dyn} and the quantities listed in column 1 restricting the dataset to events for which ΔP_{dyn} is larger than the value listed in the column labelled "Threshold". These thresholds isolate the subset of events presenting the highest correlation level of confidence for each pair of variables.

$\left.\frac{dP_{dyn}}{dt}\right\|_{\max}$	Threshold (nPa/s)	r	α
ΔV_{cl}	2.14×10^{-2}	-0.584	0.9978
$V_{cl,min}$	2.14×10^{-2}	-0.465	0.9809
Φ_{cl}	2.14×10^{-2}	-0.490	0.9870
$\overline{V}_{cl}$	2.14×10^{-2}	-0.369	0.9304
$\underline{V}_{cl}$	1.80×10^{-2}	-0.344	0.9327
$\Delta\Phi$	1.80×10^{-2}	-0.251	0.8112

Table 9. Subset thresholds and correlations for $\left.\frac{dP_{dyn}}{dt}\right|_{\max}$. The correlation coefficient r and level of confidence α of the Student test are obtained between $\left.\frac{dP_{dyn}}{dt}\right|_{\max}$ and the quantities listed in column 1 restricting the dataset to events for which $\left.\frac{dP_{dyn}}{dt}\right|_{\max}$ is larger than the value listed in the column labelled "Threshold". These thresholds isolate the subset of events presenting the highest correlation level of confidence for each pair of variables.

P_{max}	Threshold (nPa)	r	α
ΔV_{cl}	5.97	-0.526	0.9972
$V_{cl,min}$	6.14	-0.345	0.9159
Φ_{cl}	5.97	-0.334	0.9283
$\overline{V}_{cl}$	6.14	-0.256	0.7932
$\underline{V}_{cl}$	6.14	-0.266	0.8109

Table 10. Subset thresholds and correlations for P_{max}. The correlation coefficient r and level of confidence α of the Student test are obtained between P_{max} and the quantities listed in column 1 restricting the dataset to events for which P_{max} is larger than the value listed in the column labelled "Threshold". These thresholds isolate the subset of events presenting the highest correlation level of confidence for each pair of variables.

With $\Delta v_{SW}\|_{ramp}$	Threshold (km/s)	r	α
ΔV_{cl}	11.3	-0.586	0.9997
$V_{cl,min}$	11.3	-0.673	> 0.9999
Φ_{cl}	11.3	-0.638	0.9999
$\overline{V}_{cl}$	11.6	-0.692	>0.9999
$\underline{V}_{cl}$	12.0	-0.729	>0.9999

Table 11. Subset thresholds and correlations for $\Delta v_{SW}|_{ramp}$. The correlation coefficient r and level of confidence α of the Student test are obtained between $\Delta v_{SW}|_{ramp}$ and the quantities listed in column 1 restricting the dataset to events for which $\Delta v_{SW}|_{ramp}$ is larger than the value listed in the column labelled "Threshold". These thresholds isolate the subset of events presenting the highest correlation level of confidence for each pair of variables.

With Δv_{SW}	Threshold (km/s)	r	α
ΔV_{cl}	8.6	-0.541	0.9983
$V_{cl,min}$	8.6	-0.577	0.9993
Φ_{cl}	8.6	-0.614	0.9998
$\overline{V}_{cl}$	8.6	-0603	0.9997
$\underline{V}_{cl}$	8.6	-0.643	0.9999

Table 12. Subset thresholds and correlations for Δv_{sw}. The correlation coefficient r and level of confidence α of the Student test are obtained between Δv_{sw} and the quantities listed in column 1, restricting the dataset to events for which Δv_{sw} is larger than the value listed in the column labelled "Threshold". The same threshold value was found to isolate the subset of events presenting the highest correlation level of confidence for each pair of variables.

With $max\left(\frac{dv_{SW}}{dt}\right)$	Threshold (km/s^2)	r	α
ΔV_{cl}	0.222	-0.471	0.9900
$V_{cl,min}$	0.286	-0.686	0.9994
Φ_{cl}	0.286	-0.782	>0.9999
$\overline{V_{cl}}$	0.286	-0.738	0.9999
$\underline{V_{cl}}$	0.286	-0.695	0.9997

Table 13. Subset thresholds and correlations for $max\left(\frac{dv_{SW}}{dt}\right)$. The correlation coefficient r and level of confidence α of the Student test are obtained between $max\left(\frac{dv_{SW}}{dt}\right)$ and the quantities listed in column 1, restricting the dataset to events for which $max\left(\frac{dv_{SW}}{dt}\right)$ is larger than the value listed in the column labelled "Threshold".

$\Delta\|B\|$	Threshold (nT)	r	α
ΔV_{cl}	0.47	-0.724	> 0.9999
$V_{cl,min}$	0.47	-0.691	> 0.9999
Φ_{cl}	0.47	-0.676	0.9999
$\overline{V_{cl}}$	0.47	-0.678	0.9999
$\underline{V_{cl}}$	0.47	-0.724	> 0.9999

Table 14. Subset thresholds and correlations for $\Delta|B|$. The correlation coefficient r and level of confidence α of the Student test are obtained between $\Delta|B|$ and the quantities listed in column 1 restricting the dataset to events for which $\Delta|B|$ is larger than the value listed in the column labelled "Threshold". These thresholds isolate the subset of events presenting the highest correlation level of confidence for each pair of variables.

With Δv_{SW}	r	α
ΔV_{cl}	-0.554	> 0.999
$V_{cl,min}$	-0.613	> 0.999
Φ_{cl}	-0.621	> 0.999
$\overline{V_{cl}}$	-0.638	> 0.999
$\underline{V_{cl}}$	-0.678	> 0.999

Table 15. Correlation coefficients relating Δv_{SW} and several parameters describing the dynamic pressure pulse-induced flux closure, restricting the analysis to the subset for which ΔP_{dyn} > 2.8 nPa. The reported level of confidence was computed applying the Student test. A correlation coefficient of ~0.999 is found applying the Fisher test.

Figures and captions

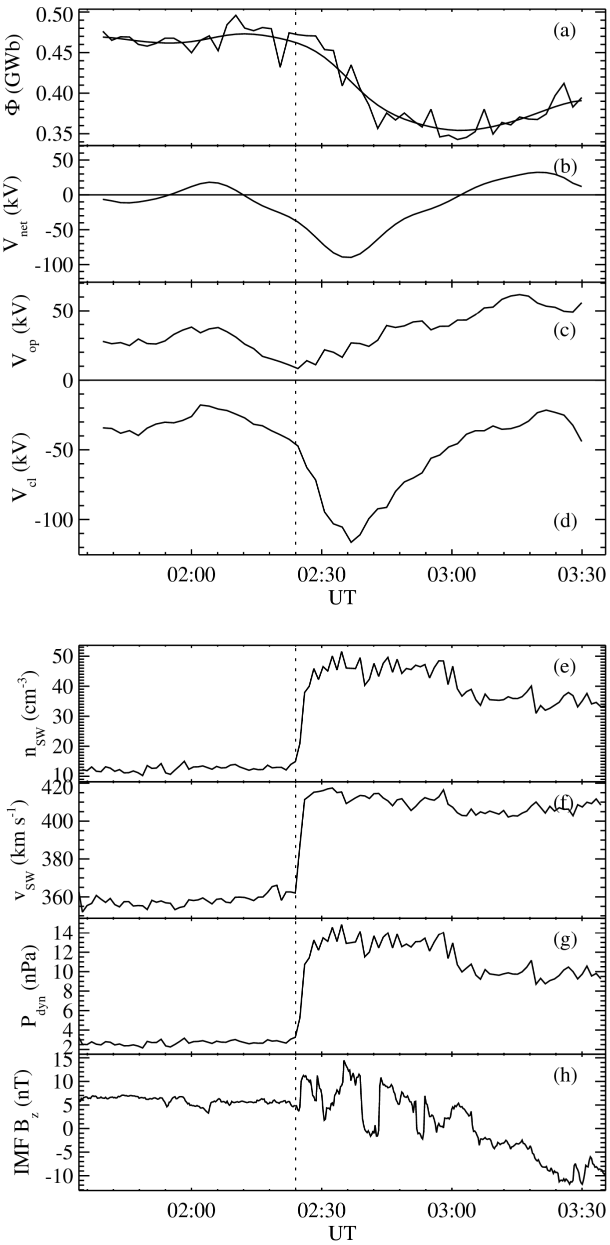

Figure 1. Dynamic pressure front recorded on 4 November 2000: The upper panel shows (a) the open magnetic flux deduced from ionospheric and auroral observations, (b) the net reconnection voltage, (c) the flux opening rate, (d) the flux closure rate. The lower panel shows solar wind data from observations of the ACE satellite (e) density, (f) velocity, (g) dynamic pressure, and (h) IMF B_z component. A suitable time shift is applied to account for propagation of the solar wind from the ACE location to the planet.

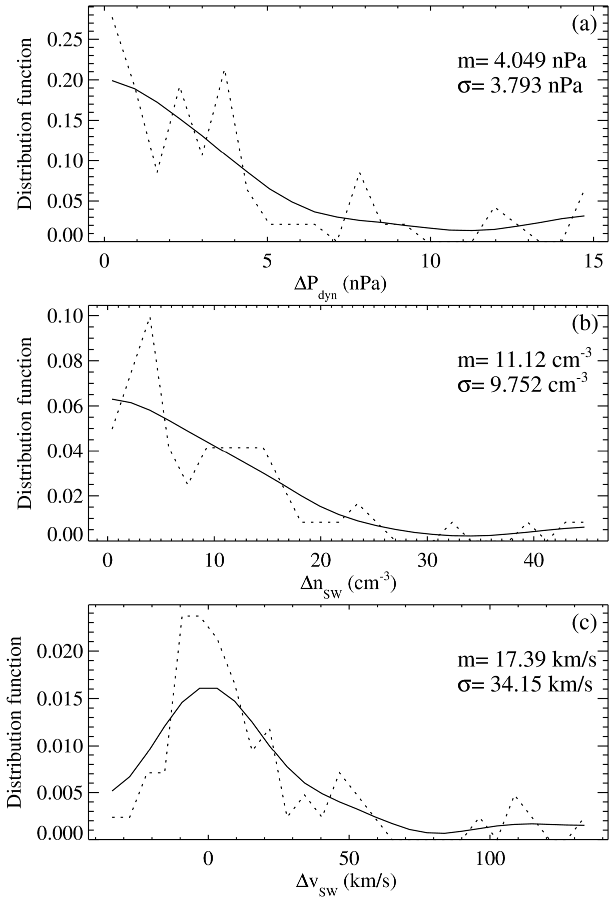

Figure 2. Statistical distribution function (dotted lines) and smoothed statistical distribution function (solid lines) of (a) the solar wind dynamic pressure variation, (b) the solar wind density variation, and (c) the solar wind velocity variation for the selected set of solar wind dynamic pressure pulses. The average and standard deviation of the sample is indicated for each variable.

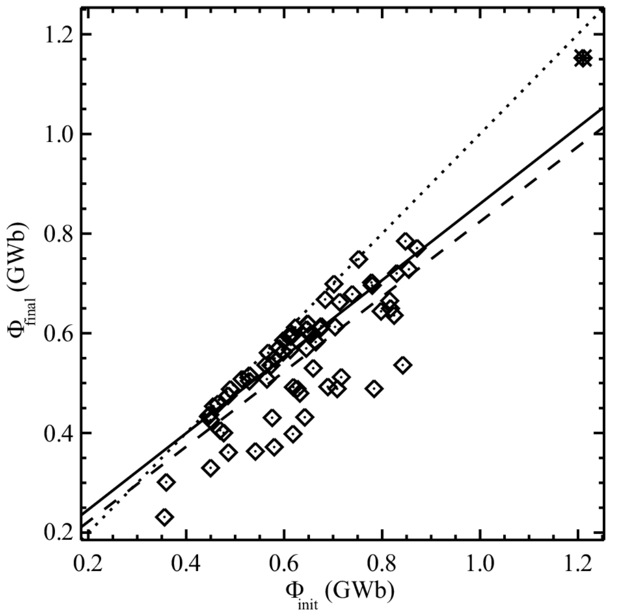

Figure 3. Final open flux as a function of the initial open flux. The data point overplotted with a * symbol is an outlier. The solid line indicates the least absolute deviation linear fit through the data points (excluding the outlier) and the dashed line is the regression line. The dotted line is the bisectrix.

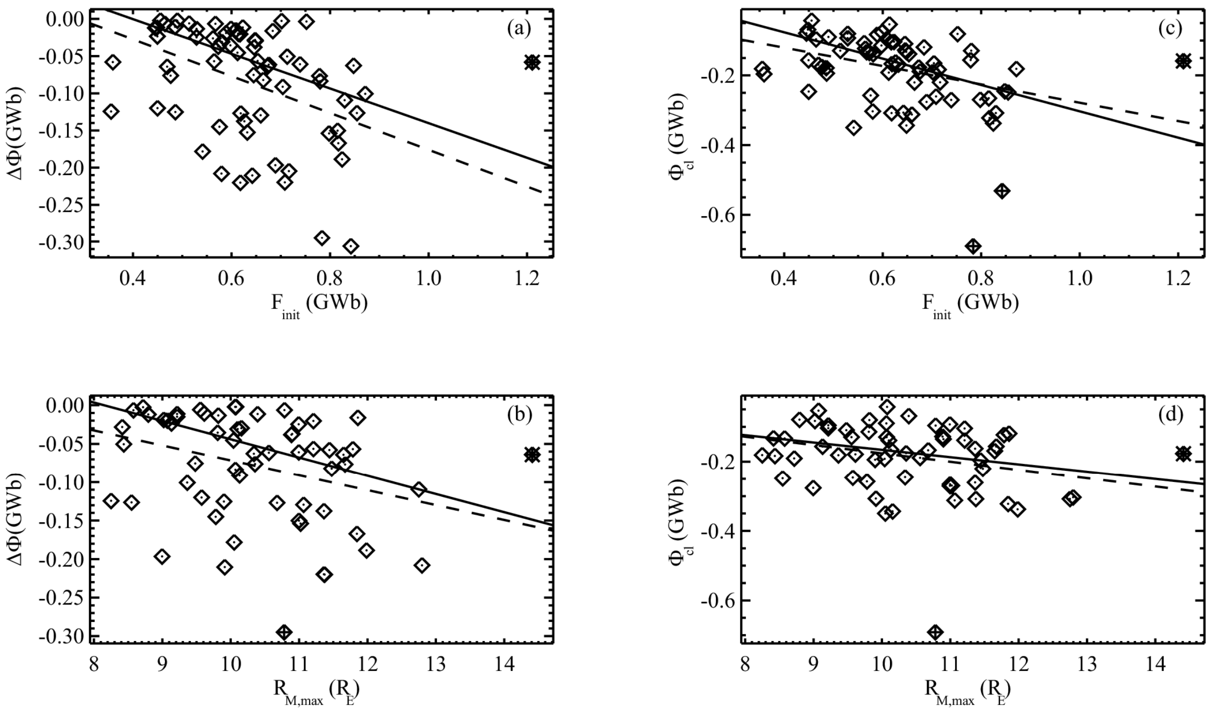

Figure 4. Open flux variation ($\Delta\Phi$) as a function of the initial open flux Φ_{init} (a) and maximum magnetopause radius $R_{M,max}$ expressed in earth radii (b). Total amount of magnetic flux closed Φ_{cl} as a function of the initial open flux Φ_{init} (c) and maximum magnetopause radius $R_{M,max}$ (d). Data points overplotted with a * or a + symbol are outliers. The solid lines are the least absolute deviation linear fits through the data points (excluding the outliers) and the dashed lines are the regression lines.

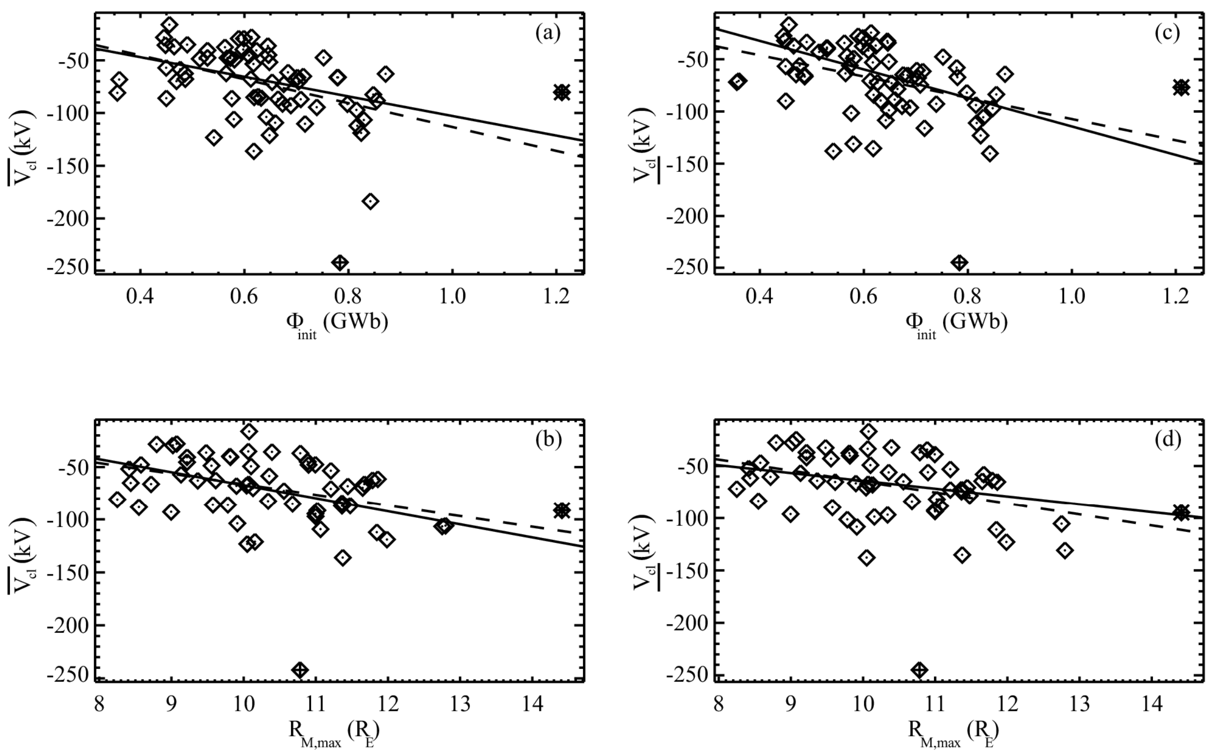

Figure 5. (a) Average closure voltage $\overline{V_{cl}}$ as a function of the initial open flux Φ_{init} and (b) the maximum magnetopause radius $R_{M,max}$ expressed in earth radii, (c) median closure voltage $\underline{V_{cl}}$ versus the initial open flux Φ_{init} and (d) maximum magnetopause radius $R_{M,max}$ (d). Data points overplotted with a * or a + symbol are outliers. The solid lines are the least absolute deviation linear fits through the data points (excluding the outliers) and the dashed lines are the regression lines.

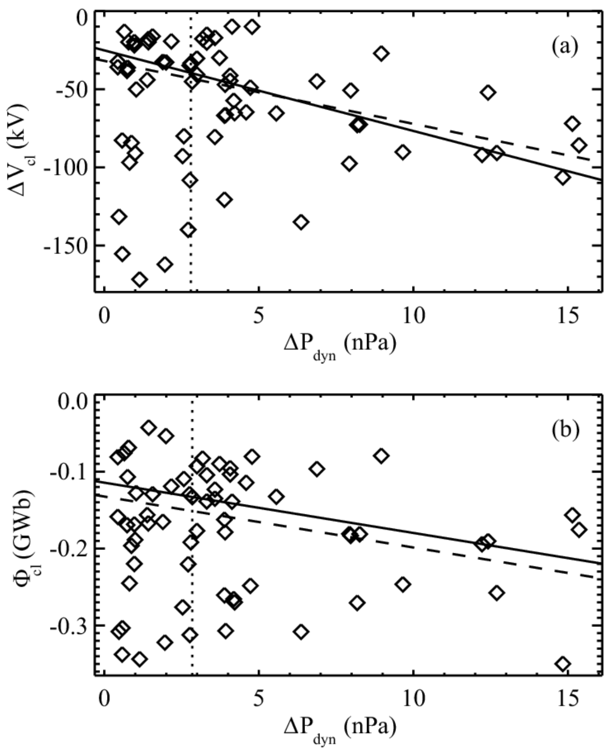

Figure 6. Closure voltage intensification (a) and amount of open flux closed (b) versus the solar wind dynamic pressure increase. The dotted vertical lines indicate a threshold of ~2.8 nPa, the solid and dashed lines are least absolute deviation fits and regression lines, respectively, through the data subset satisfying $\Delta P_{dyn} > 2.8$ nPa.

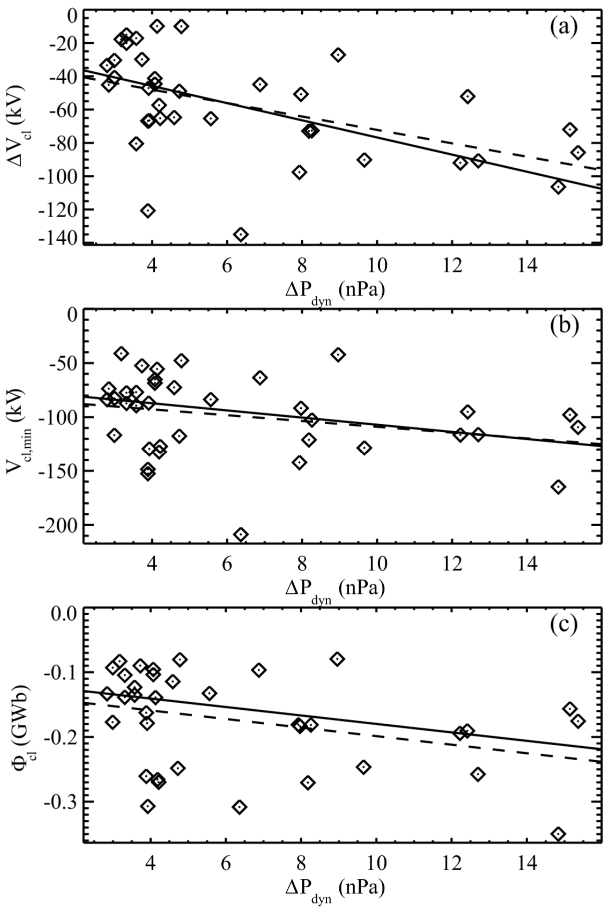

Figure 7. Closure voltage variation ΔV_{cl} (top panel), minimum closure voltage $V_{cl,min}$ (middle panel) and total amount of flux closed Φ_{cl} (bottom panel) as a function of the solar wind dynamic pressure increase ΔP_{dyn}, for the subset of events for which ΔP_{dyn} > 2.8 nPa. Outliers were not plotted. The solid lines represent the least absolute deviation fits through the data.

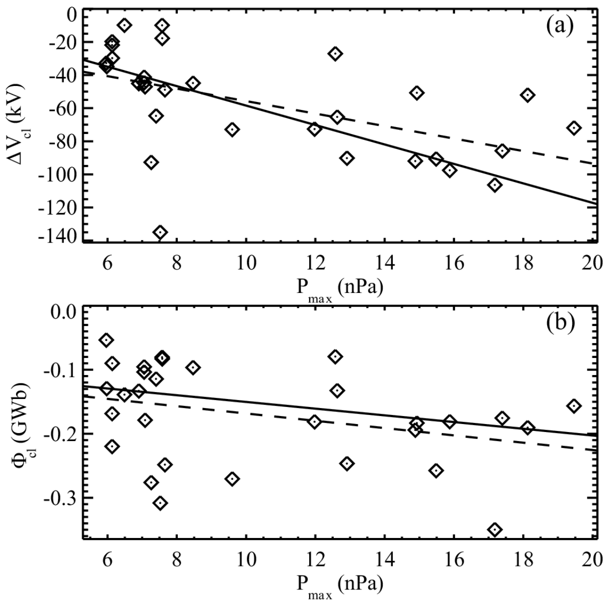

Figure 8. (a) Closure voltage variation ΔV_{cl}, and (b) total amount of flux closed Φ_{cl} as a function of the maximum solar wind dynamic pressure reached in each event $P_{dyn,max}$, for the subset of events for which $P_{dyn,max} > 5.97$ nPa. Outliers are not plotted. The solid lines represent the least absolute deviation fits through the data, and the dashed lines are the regression lines.

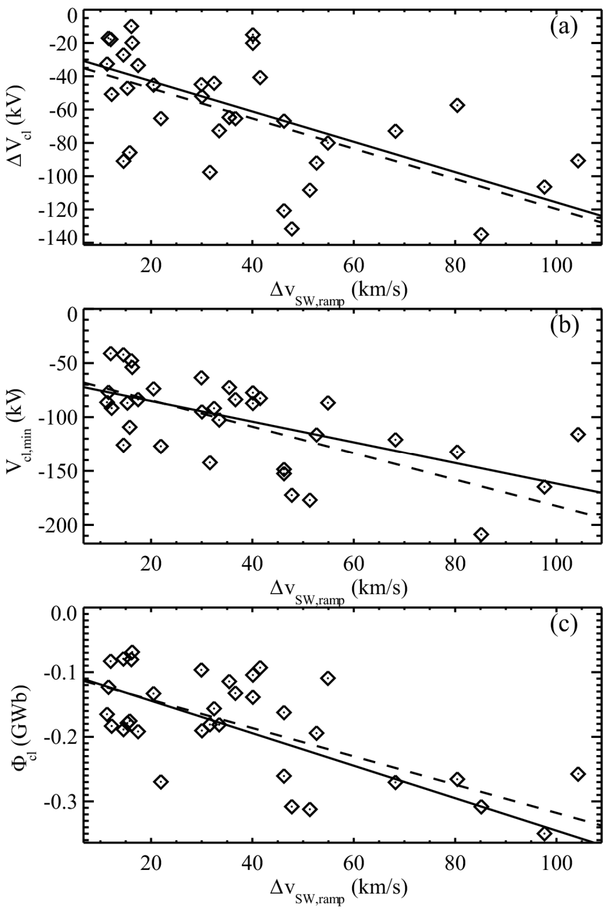

Figure 9. (a) Closure voltage variation ΔV_{cl}, (b) minimum closure voltage $V_{cl,min}$ and (c) total amount of flux closed Φ_{cl} as a function of the solar wind velocity variation during the ramp of the solar wind dynamic pressure pulse, for the subset of events for which $\Delta v_{SW,ramp} > 11.3$ km/s. Outliers are not plotted. The solid lines represent the least absolute deviation fits through the data, and the dashed lines are the regression lines.

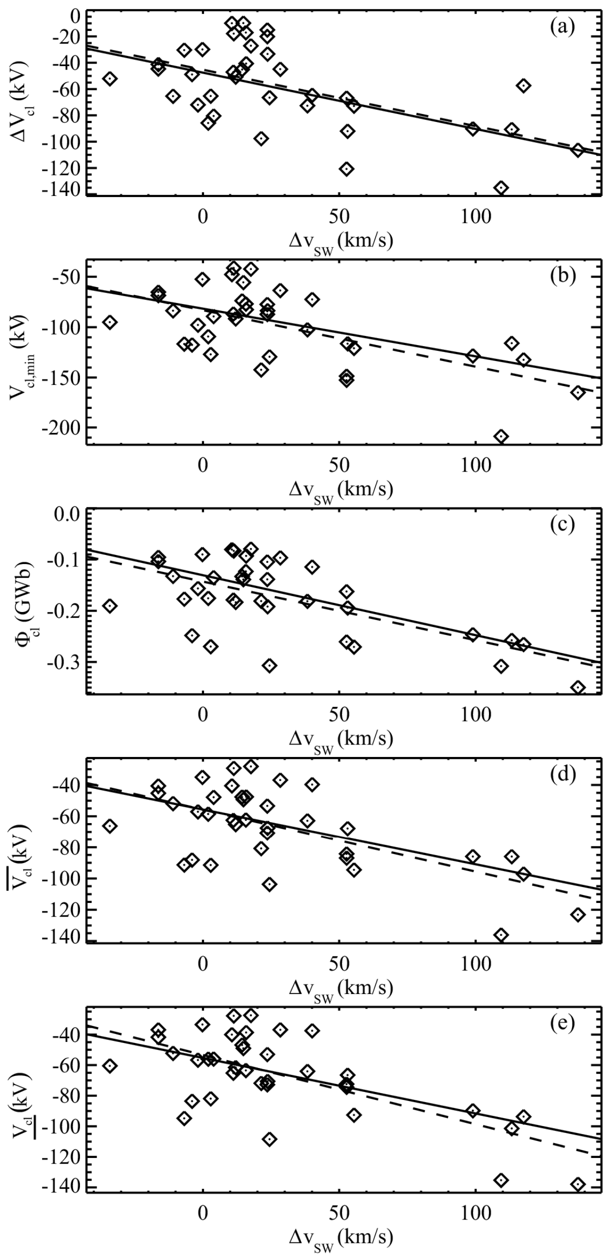

Figure 10. (a) Closure voltage variation ΔV_{cl}, (b) minimum closure voltage $V_{cl,min}$, (c) total amount of flux closed, (d) average closure voltage $\overline{V_{cl}}$, and (e) median closure voltage $\underline{V_{cl}}$ versus the variation of the solar wind velocity Δv_{SW}, for the subset of events for which the variation of the solar wind dynamic pressure is $\Delta P_{dyn} > 2.8$ nPa. Outliers are not plotted. The solid lines represent the least absolute deviation fits through the data, and the dashed lines are the regression lines.

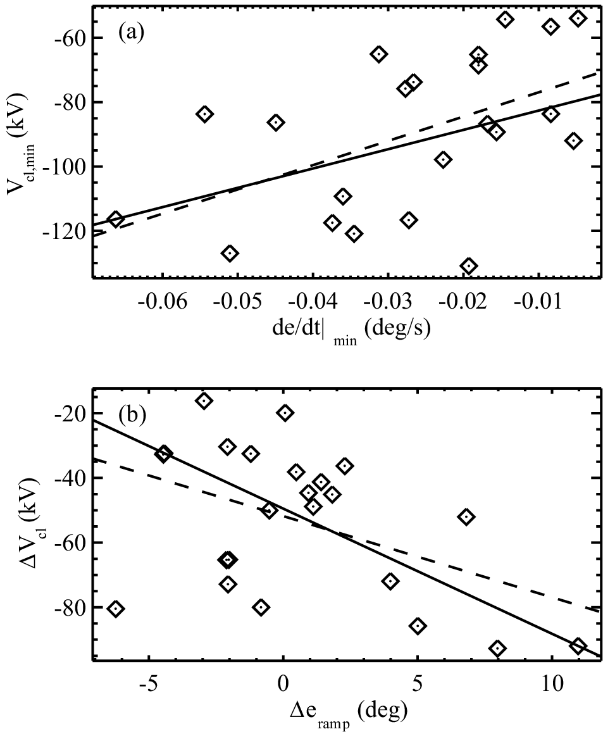

Figure 11. (a) Minimum closure voltage versus the minimum rate of change of the elevation angle deduced from GOES-8 measurements, and (b) the closure voltage intensification versus the variation of the elevation angle during the ramp of the solar wind dynamic pressure pulse, deduced from GOES-8 measurements. The solid lines are the least absolute deviation fits to the data, and the dashed lines are the regression lines. Outliers are not plotted.